SAGO PALM 28: 22 – 28 (2020)

Conical Projection Measurement of Sago Palm (*Metroxylon sagu* Rottb.) Phytoliths in Leyte, Philippines

Masanori Okazaki[1,*], Mitsuhisa Baba[2], Toshihiko Momose[3],
Marcelo A. Quevedo[4] and Ma. Kristine L. Aban[4]

[1]Japan Soil Research Institute, Inc., 3-26-4, Yatocho, Nishitokyo, Tokyo 188-0001 Japan

[2]Kitasato University, 35-1, Higashinijusanbanncho, Towada, Aomori 034-8628 Japan

[3]Ishikawa Prefectural University, 1-308, Suematsu, Nonoichi, Ishikawa 921-8836 Japan

[4]Philippine Rootcrops Research and Training Center (PhilRootcrops), Visayas State University, Leyte, Philippines

*Corresponding author: Japansoilco_okazaki@mbr.nifty.com

Abstract: The palm family generally has characteristic phytoliths with many conical projections. Diagnostic, amorphous spheroid, echinate phytoliths are present in all organs of the sago palm (*Metroxylon sagu* Rottb.), which constitute approximately 8–9% of leaflet dry weight. For phytolith observation, transmitted-light (TLM) and scanning electron microscopy (SEM) were used at x400 and x1000 magnifications. The terminal angles and length of conical projections were calculated according to Heron's formula. The mean maximum diameter of phytoliths and the mean number, mean terminal angle, and mean length of conical projections of *M. sagu* were 13.2 μm, 26.0, 84.0°, and 0.54 μm, respectively, under TLM. Meanwhile, the phytoliths of *M. sagu* were 15.1 μm of the mean maximum diameter of phytoliths, 21.6 of the mean number of conical projections, 91.4° of the mean terminal angle of conical projections, and 1.45 μm of the conical projection lengths under SEM. It is possible to utilize spheroid echinate morphology, conical projections arranged at the periphery, and terminal angles and lengths of conical projections as indicators of the identification of *M. sagu* phytoliths.

Keywords: conical projection, echinate, light-transmitting microscope, phytolith, scanning electron microscope, spheroid, Heron's formula

Introduction

Silicon (Si) is effective in controlling various pests and diseases caused by both fungi and bacteria in different plant species (Ma, 2004), which alleviates various abiotic stresses, including salt stress, metal toxicity, drought stress, radiation damage, nutrient imbalance, high temperature stress, and freezing stress (Mitani and Ma, 2005). Various plants form distinctive phytoliths by the uptake of Si from the soil (Ryan, 2014). Takahashi and Miyake (1976a) reported the silicon content in land plants. Hodson et al. (2005) also showed phylogenetic variation in the silicon composition of plants from 54 papers. Phytoliths—mainly spheroid echinate morphotypes—are abundantly produced in palms (Albert et al., 2009). Benvenuto et al. (2015) described globular phytoliths in 10 species of *Arecaceae*, four species of *Bromeliaceae*, 10 species of *Cannaceae*, one species of *Marantaceae*, three species of *Orchidaceae*, one species of *Strelitziaceae*, and one species of *Zingiberaceae* from Argentina. *Metroxylon sagu* Rottb. was not included in their *Arecaceae* families studied. Morcote-Ríos et al. (2016) surveyed phytoliths in 92 species of Amazonian palms, representing 29 genera across four subfamilies. However, they did not describe *M. sagu* phytoliths because the Amazon is far from the

M. sagu–growing area.

M. sagu is able to absorb and accumulate Si in all organs and finally form phytoliths as biogenic amorphous opal silica ($SiO_2 \cdot nH_2O$), which shows high durability (Baba et al., 2020). Fenwick et al. (2011) tried to discriminate between four (*Areca catechu* L., *Calamus aruensis* Becc., *Cocos nucifera* L., and *M. sagu*) palm phytoliths on Watom Island, Papua New Guinea, using several parameters, such as the maximum diameter of phytolith, perpendicular diameter, number of conical projections, conical projection length, and conical projection angle. They showed that there were statistically significant differences between the leaf phytoliths of *Areca catechu*, *Calamus aruensis*, *Cocos nucifera*, and *M. sagu*. The maximum diameter of phytolith, perpendicular diameter of phytolith, number of conical projections, and conical projection length of *M. sagu* were determined and can be used for discriminating between the four palms. The distinguishable mean conical projection length of M. sagu indicated was 1.1 μm (Fenwick et al., 2011). On Easter Island (Rapa Nui), Bowdery (2015) found M. sagu phytoliths in 0.97 m horizon (KA 5005-3A), which corresponded to a Cal age between AD 1394–1425 and AD 1634–1672. The combination study of phytolith assemblage and ^{14}C dating contributes to the fields of archaeology as well as vegetation and food science.

The objectives of this study are to show spheroid echinate phytoliths in *M. sagu* leaflets using TLM and SEM and to evaluate several variables of phytolith morphologies of *M. sagu* growing in the Philippines in order to clearly identify *M. sagu* phytoliths and to propose a technology for identifying *M. sagu* by an index of the terminal angle and the length of conical projections.

Materials and Methods

1. Sago palm and leaflet phytolith preparation

Sago palms in Pangasugan, Leyte, Philippines (Fig. 1) were approaching flowering stage (11 years after transplanting, hit by Typhoon Yolanda in 2013), and the eleventh living leaf from the palm apex was taken in 2016. *M. sagu* generally accumulates spheroid echinate phytolith assemblage in leaflets. For the observation and counting of phytolith samples, the leaflets were washed with distilled water to remove contaminants. They were air-dried and incinerated in an electric furnace at 500 °C for 4 hours according to a method modified from those of Hodson et al. (2005) and Benvenuto et al. (2015).

Fig 1. Sago palm (*Metroxylon sagu* Rottb.) field in Pangasugan, Leyte, Philippines

2. Incinerated leaflet samples and X-ray diffraction

Phytoliths in incinerated leaflets, dried after treatment with 0.01 M HCl and washing with distilled water three times, were evaluated as the dry weight percentage of leaflets. In order to show amorphous *M. sagu* phytoliths and the chemical bonding of silicon to other elements in phytoliths, X-ray diffraction of the incinerated leaflet samples was provided on an antireflection silicon sample holder because of its exclusion of external X-ray intensities when using an X-ray diffractometer (Rigaku, Miniflex). Copper (Cu) Kα radiation was used with a nickel filter. The scanning speed was recorded as 2° min^{-1}, and the operation angle was 3° to 60° for 2θ.

3. Parameter measurement of sago palm phytoliths

After gravitational sedimentation extraction, the dried leaflet phytolith samples were mounted onto

slides using a suitable permanent fixative (Matsunami, MGK-S). Phytolith parameters were observed and measured by TLM (Meiji Techno, MT-5000) and SEM (Hitachi Miniscope, TM-1000). The mean diameter of phytoliths and the number of conical projections were measured by photographs of LTM at x400 magnification and SEM at x400 and x1000 magnification. The length of conical projections at the edge portion was measured. The terminal angle of conical projections may regulate the number of diagnostic conical projections. The terminal angle of conical projections was calculated by the length of the triangle's sides based on Heron's formula.

$S = \sqrt{s(s-a)(s-b)(s-c)}, s = \frac{a+b+c}{2},$

if $a \geq b, c$ $h = 2S/a, B = \sin^{-1} h/c, C = \sin^{-1} h/b$

if $b \geq c, a$ $h = 2S/b, C = \sin^{-1} h/a, A = \sin^{-1} h/c$

if $c \geq a, b$ $h = 2S/c, A = \sin^{-1} h/b, B = \sin^{-1} h/a$

$A + B + C = 180,$

where S is the area of the triangle; h is the triangle's height; A, B, and C are angles; and a, b, and c are the triangle's sides.

Figure 2 shows a drawing of spheroid echinate and conical projections accompanied by Heron's formula, which can calculate the angle and length of conical projections from three sides of a triangle.

Results

1. Content of phytoliths in sago palm leaflets

The mean weight of incinerated *M. sagu* leaflet samples, comprised of phytoliths, a small amount of charcoal, and others, is 8.7 ± 3.7% of the dry leaflet matter (Table 1). This is comparable to the intermediate value of Si content (5 to 15% of leaf dry matter) in *Gramineae* phytolith, as represented by Kondo and Sase (1986). Takahashi and Miyake (1976a) found large variation of Si content in leaf blades, with respect to 62 species of monocotyledons (0.01 to 6.3%), including four species of *Arecaceae* (0.27 to 1.41%). Takahashi and Miyake (1976b) also showed 0.02 to 0.77% of Si content in leaf blades with regard to 85 dicotyledon species. Furthermore, Takahashi et al. (1981a, b) reported 3.42 to 11.82% of

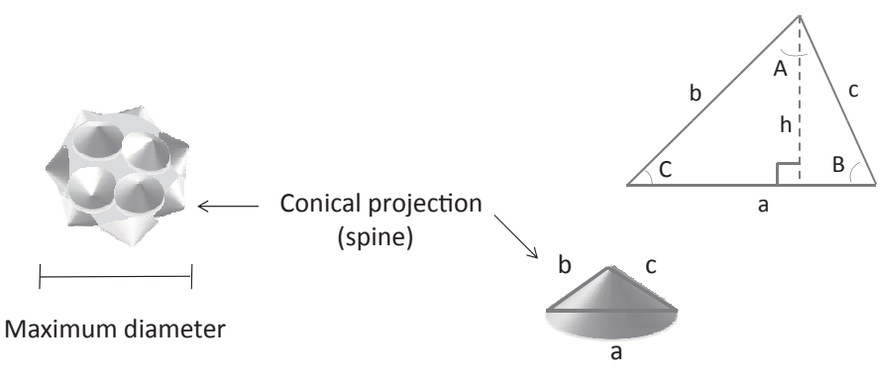

Fig 2. Drawing of spheroid echinate morphotype and angles/sides of Heron's formula

a , b and c : sides

A, B and C : angles

h: the height of the triangle = the length of the conical projection

Table 1. Incinerated sample weight of *Metroxylon sagu* leaflet

	Dry weight of incinerated sample (%)
Metroxylon sagu	8.7 ± 3.7

n = 27

Si content in leaf blades with respect to 70 species of *Gramineae* and 0.11 to 4.68% of Si content in *Commelinales*, including *Cyperales*, *Urticaceae*, and *Cucurbitaceae*. The content of Si in *M. sagu* leaflets, therefore, corresponded to the median value of Si content in *Gramineae*.

2. X-ray diffraction pattern of *M. sagu* phytoliths

X-ray diffraction of *M. sagu* phytoliths shows an amorphous pattern with a wider peak from 20 to 30 degrees 2 θ for Cu Kα (Fig. 3), which corresponds to the result of bamboo phytolith by Klinowski et al. (1998). Nevertheless, the appearance of *M. sagu* phytoliths revealed graceful shapes of spheroid echinates. Although this diffraction pattern is similar to that of quartz glass SiO_2, which has its peak around 22 degrees, it reveals the weak bias to the higher range region when affected by four coordination number ions, likewise Li. When affected by six coordination number ions, such as sodium, calcium, magnesium, and barium, a strong bias was found in the peak, providing a decreasing peak and/or unclear peak (Ando, 1961).

3. Microscope observation

Under TLM, the phytolith assemblage of *M. sagu* represents diagnostic spheroid echinate (Madella et al., 2005; Neumann et al., 2019) morphologies (Fig. 4). According to the description of Morcote-Ríos et

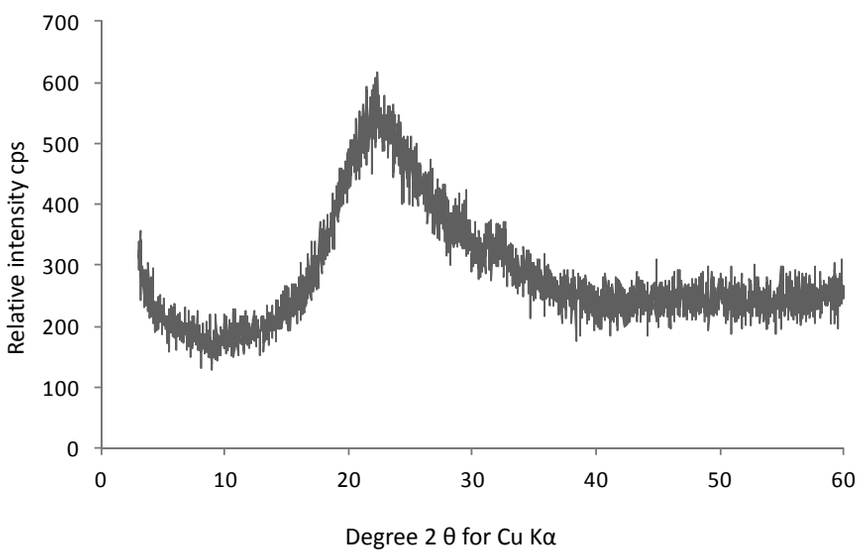

Fig 3. X-ray diffraction pattern of *M. sagu* phytolith

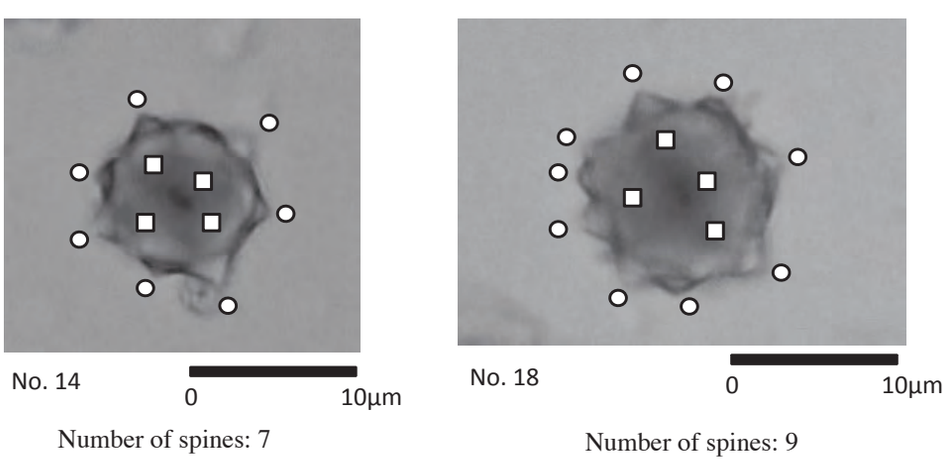

Fig 4. TLM images of *M. sagu* phytoliths

○ : top of conical projection measured for conical projection length
□ : top of conical projection unmeasured for conical projection length

al. (2016), *M. sagu* presented acute conical projections symmetrically arranged at the periphery, 15–30 peripheral projections, of which the mean maximum diameter is 4–20 nm, consistent with the reports of Fenwick et al. (2011) and Bowdery et al. (2015). SEM images showed much acuter conical projections at the periphery (Fig. 5).

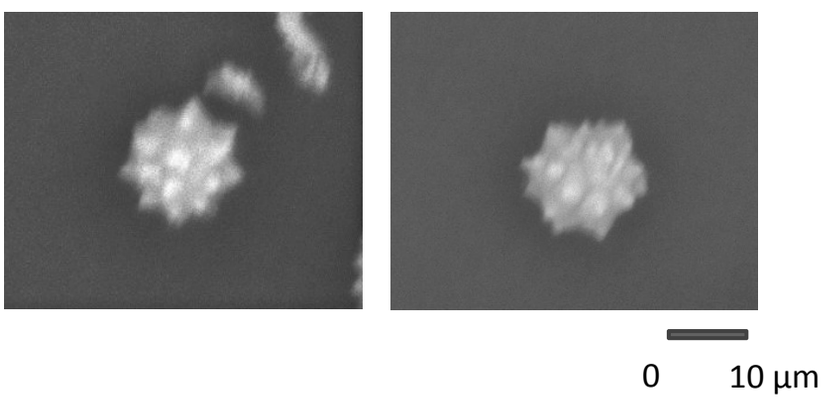

Fig 5. SEM images of *M. sagu* phytoliths

From both images of TLM and SEM, we determined the mean maximum diameter of phytoliths, number of conical projections, terminal angle, and length of conical projections (Table 2). The mean maximum diameter of *M. sagu* phytoliths was 13.2 ± 1.6 μm. The mean number of conical projections was 26.0 ± 3.2. The mean terminal angle and length of conical projections were 84.0 ± 10.0° and 0.54 ± 0.21 μm, respectively, under TLM. Meanwhile, the mean maximum diameter of *M. sagu* phytoliths was 15.1 ± 2.6 μm. The mean number of conical projections was 21.6 ± 6.2. The mean terminal angle and length of conical projections were 91.4 ± 11.3 ° and 1.45 ± 0.66 μm, respectively, under SEM. The mean maximum diameter determined with SEM tended to be larger than those determined with LTM.

Table 2. Variables of *Metroxylon sagu* phytoliths

Microscope	Mean maximum diameter (μm)	Number of conical projection	Terminal angle (°)	Length of conical projection (μm)
TLM	13.2 ± 1.6	26.0 ± 3.2	84.0 ± 10.0	0.54 ± 0.21
SEM	15.1 ± 2.6	21.6 ± 6.2	91.4 ± 11.3	1.45 ± 0.66

TLM: transmitted-light microscope

SEM: scanning electron microscope

n = 10

Discussion

Phytoliths are formed in plants and take on the size and shape of the compartment where they are deposited, varying between types, different organs within a plant, and different plant species (Leng et al., 2009). It is possible to identify *M. sagu* phytoliths based on morphotype: size, shape, margins, surface texture, and ornamentation. *M. sagu* leaflets have solid spheroidal phytoliths with conical projections distributed over the entire surface. The conical projections of *M. sagu* vary in size and are simple individually, larger, and more closely distributed on the surface than those of other palms provided by Neumann et al. (2019). From the X-ray diffraction analysis in this study, *M. sagu* phytoliths including conical projections contained six coordination numbers of ions in the phytolith SiO_2 structure.

Silica polymerization reaction occurs within the silica deposition vesicle, which is suggested to be acidic (Verieling et al., 1999) and is controlled by a combination of silaffin proteins and polyamines, although several reports of silica polymerization were found in diatoms (Sumper and Kröger, 2004). Accordingly, phytoliths occlude carbon (proteins and amines) in their structure (Alexandre et al., 2015). Incineration at 500 °C for 3 h (Morcote-Ríos et al., 2016) has been used for the extraction of phytoliths from *M. sagu* leaflets, which provides chars from occluded carbon in the phytolith structure. When using TLM for identification, it is important to remember that incineration may give rise to char produced from occluded carbon, resulting in a darker center in the phytolith. On the other hand, because of its deeper focus, SEM can supply explicit images of conical projections. As a result, there was a tendency that the mean length of conical projections with SEM was longer than that with TLM. It is noted that we are able to use an analytical method favorable to the identification and measurement of phytolith variables.

Conclusion

Phytoliths of *M. sagu* are abundantly present in leaflets. Since phytoliths of *M. sagu* have distinguishable, diagnostic spheroid echinate characteristics, they can be successfully identified using TLM and SEM, based on the purpose of the research. The determination of the number, terminal angle, and length of conical projections is effective for the identification of *M. sago* phytoliths.

Acknowledgment: We appreciate Professor Emeritus Yoshiro Kato, Shizuoka University, for identifying the primary minerals and phytoliths.

References

Albert, R. M., M. K. Bamford and D. Cabanes 2009 Palaeoecological significance of palms at Olduvai Gorge, Tanzania, based on phytolith remains. Quaternary International 193: 41-48.

Alexandre, A., I. Basile-Doelsch, T. Delhaye, D. Borshneck, J. C. Mazur, P. Reyerson and G. M. Santos 2015 New highlights of phytolith structure and occluded carbon location: 3-D X-ray microscopy and NanoSIMS results. Biogeosciences 12: 863-873.

Ando, J. 1961 X-ray Diffraction patterns of a variety of glasses. Journal of the Ceramic Association, Japan 11: 380-383 (in Japanese)

Baba, M., M. Okazaki, M., K. Nakaie, T. Momose, M. A. Quevedo and S. B. Lina 2020 Phytoliths in Sago Palm (*Metroxylon sagu* Rottb.) from Pangasugan, Leyte, Philippines. Sago Palm 28: 5-11.

Benvenuto, M. L., M. F. Honaine, M. L. Osterrieth and E. Morel 2015 Differentiation of globular phytoliths in *Arecaceae* and other monocotyledons: morphological description for paleobotanical application. Turkish Journal of Botany 39: 341-353.

Bowdery, D. 2015 An enigma revisited: identification of palm phytoliths extracted from the 1983 Rapa Nui, Aano Kao2 core. Vegetation History and Archaeobotany 24: 455-466. doi: 10.1007/s00334-014-0503-x

Fenwick, R. S. H., J. Carol, J. Lentfer and M. I. Weisler 2011 Palm reading: a pilot study to discriminate phytoliths of four *Arecaceae* (Palmae) Taxa. Journal of Archaeological Science 38: 2190-2199.

Hodson, M. J., P. J. White, A. Mead and M. R. Broadley 2005 Phylogenetic variation in the silicon composition of plants. Annual of Botany, 96: 1027-1046

Klinowski, J., C-F. Cheng, J. Sanz J. M. Rojo and A. L. Mackay 1998 Structural studies of tabasheer, an opal of plant origin. Philosophical Magazine A 77: 201-216.

Kondo R. and T. Sase 1986 Opal phytoliths, their nature and application. The Quaternary Research 25: 31-63.

Leng, M. J., G. E. AQ. Swann, M. J. Hodson, J. J. Tyler, S. V. Patwardhan and H. J. Sloane 2009 The

potential use of silicon isotope composition of biogenic silica as a proxy for environmental change. Silicon 1: 65-77.

Ma, J. F. 2004 Role of silicon in enhancing the resistance of plants to biotic and abiotic stresses. Soil Science and Plant Nutrition, 50: 11-18

Madella, M., A. Alexandre and T. Ball 2005 International code for phytolith nomenclature 1.0. Annals of Botany 96: 253–260.

Mitani, N. and J. F. Ma 2005 Uptake system of silicon in different plant species. Journal of Experimental Botany 56: 1255-1261.

Morcote-Ríos, G., R. Bernal and L. Raz 2016 Phytoliths as a tool for archaeobotanical, palaeobotanical and palaeoecological studies in Amazonian palms. Botanical Journal of the Linnean Society, 182: 348-360.

Neumann, K., C. A. E. Strömberg, T. Ball, R. M. Albert, L. Vrydaghs and L. S. Cummings 2019 International code for phytolith nomenclature (ICPN) 2.0. Annals of Botany 20: 1–11.

Ryan, P. 2014 Phytolith studies in archaeology, In The Archaeological Record, ed. by C. Smith, p. 5920-5931, Springer, Springer Science+Business, Media New York 2014 https://www.researchgate.net/publication/265219031_Phytolith_Studies_in_Archaeology

Sumper, M. and N. Kröger 2004 Silica formation in diatoms: the function of long-chain polyamines and silaffins. Journal of Materials Chemistry 14: 2059-2065.

Takahashi, E. and T. Miyake 1976a Distribution of silica accumulator plants in the plant kingdom, (1) Monocotyledons, Comparative studies on the silica nutrition in plants (Part 5). Japanese Society of Soil Science and Plant Nutrition (Journal of the Science of Soil and Manure, Japan) 47: 296-300. (in Japanese)

Takahashi, E. and T. Miyake 1976b Distribution of silica accumulator plants in the plant kingdom, (2) Dicotyledons, Comparative studies on the silica nutrition in plants (Part 6). Japanese Society of Soil Science and Plant Nutrition (Journal of the Science of Soil and Manure, Japan) 47: 301-306. (in Japanese)

Takahashi, E., T. Tanaka and T. Miyake 1981a Distribution of silica accumulator plants in the plant kingdom, (5) Gramineae (Graminales), Comparative studies on the silica nutrition in plants (Part 14). Japanese Society of Soil Science and Plant Nutrition (Journal of the Science of Soil and Manure, Japan), 52: 503-510. (in Japanese)

Takahashi, E., T. Tanaka and T. Miyake 1981b Distribution of silica accumulator plants in the plant kingdom, (6) Commelinales, Cyperales and some dicotyledoneae families (Cucurbitaceae and Urticaceae), Comparative studies on the silica nutrition in plants (Part 15). Japanese Society of Soil Science and Plant Nutrition (Journal of the Science of Soil and Manure, Japan) 52: 511-515. (in Japanese)

Vrieling, E. G., W. W. C. Gieskes and T. P. M. Beelen 1999 Silicon deposition in diatoms: Control by the pH inside the silicon deposition vesicle. Journal of Phycology 35: 548-559.